

# Optical control of collective states in 1D ordered atomic chains beyond the linear regime

N. Fayard,\* I. Ferrier-Barbut, A. Browaeys, and J.-J. Greffet  
*Université Paris-Saclay, Institut d'Optique Graduate School,  
CNRS, Laboratoire Charles Fabry, 91127 Palaiseau, France*  
(Dated: May 29, 2023)

Driven by the need to develop efficient atom-photon interfaces, recent efforts have proposed replacing cavities by large arrays of cold atoms that can support subradiant or superradiant collective states. In practice, subradiant states are decoupled from radiation, which constitutes a hurdle to most applications. In this work, we study theoretically a protocol that bypasses this limit using a one dimensional (1D) chain composed of  $N$  three-level atoms in a V-shaped configuration. Throughout the protocol, the chain behaves as a time-varying metamaterial: enabling absorption, storage and on-demand emission in a spectrally and spatially controlled mode. Taking into account the quantum nature of atoms, we establish the boundary between the linear regime and the nonlinear regime. In the nonlinear regime, we demonstrate that doubly-excited states can be coherently transferred from superradiant to subradiant states, opening the way to the optical characterization of their entanglement.

## I. INTRODUCTION

The atoms' ability to store and process quantum information combined with the minimal loss through light propagation make atom-photon platforms prime candidates for realizing scalable quantum networks [1–3]. In practice, it is necessary to enhance the light-matter interaction in order to enable the transfer of the information between the atoms and the photons [4]. To this aim, one possibility consists in interfacing atoms to cavities [5–9], nanofibers [10–13] or photonic crystal waveguides [14–19] which results in quasi one dimensional spontaneous emission [20] and increased light-matter interaction. Those features triggered a variety of theoretical proposals for applications in quantum optics and many-body physics [21, 22]. As of today, most of their experimental realizations have remained elusive in the many-body regime due the difficulty of interfacing efficiently a large number of atoms with nanostructures [23].

Recently, it has been shown that strong light-matter interaction can also emerge in large arrays of atoms assembled in free-space [24–27]. Indeed, when the interatomic distance is reduced below the wavelength, the light-induced interaction between atoms becomes strong enough to alter the modes of the atomic array which behaves as a metasurface. As a result, some of the modes become superradiant [28–34] and are associated with an enhanced radiation rate while others become subradiant [35–39] and are decoupled from the radiation. From an experimental point of view, the ability to create large arrays of neutral atoms with  $\mu\text{m}$  interatomic distances has already been demonstrated in order to perform quantum simulations [40–43]. However, the reduction of the atomic distance below the wavelength is extremely challenging [27, 44]. For this purpose, we consider a platform

composed of 3-levels atoms in a V-shaped configuration. The role of the second transition is dual. First, it enables the optical trapping of the atoms with interatomic distances sufficiently small such that subradiance emerges. Second, it permits the local manipulation of the atomic transition frequencies using light shifts and address the subradiant modes of the array [27, 38] as proposed recently [45, 46]. So far, those theoretical studies have considered the interaction of atoms with single photons so that a classical scattering description is valid. Motivated by the possibility to implement this scheme in ongoing experiments using Sr, Yb and Dy [47, 48], we study theoretically a similar protocol for a 1D atomic chain and go beyond the linear regime. This enables the exploration of the onset of the many-body regime, where non-linear effects appear. It also permits the description of the illumination of the chain by an intense coherent pulse. Taking advantage of these possibilities, we present a method to: (i) excite the most superradiant singly-excited state of the chain from the far field with an intense coherent pulse, (ii) transfer the excitation to the most subradiant state using a position varying detuning (PVD), (iii) store the excitation, and (iv) emit the photon in the *desired* superradiant mode of the chain, thus controlling its frequency, its emission rate and pattern.

Our theoretical analysis is valid beyond the linear regime and reveals that the doubly-excited population follows a similar trajectory than the singly-excited one. In particular, we demonstrate that we can transfer the two-photon population at will into its most subradiant form where it can be stored and studied.

## II. DESCRIPTION OF THE SYSTEM

In this work, we explore a simple and robust physical system that could be built in a lab capable of absorbing, storing and emitting a photon with a temporal and spatial control. It consists in a linear chain of atoms with a

---

\* Corresponding author: nikos.fayard@institutoptique.fr

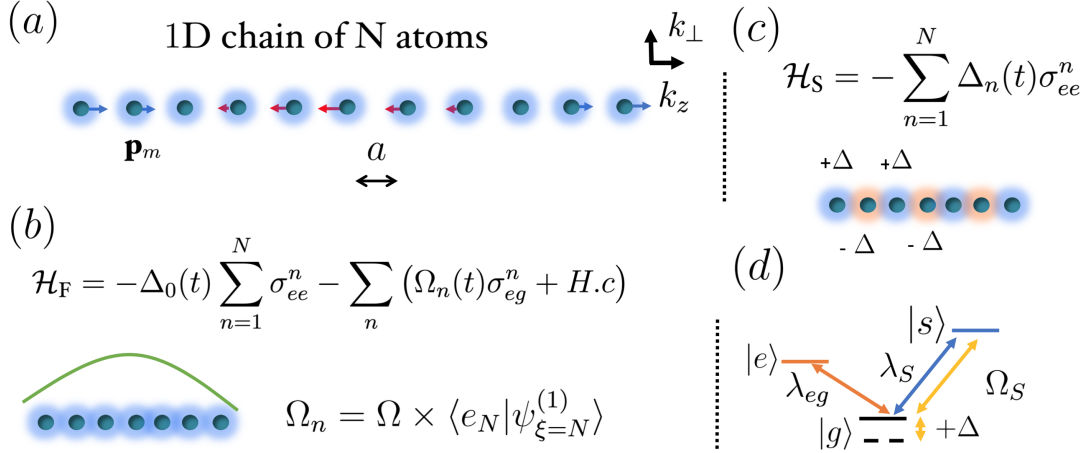


FIG. 1. a) Scheme of a 1D atomic chain composed of  $N$  atoms at positions  $\mathbf{r}_m = (0, 0, ma)$  and represented with a polarization linear and parallel to the chain  $\mathbf{p}_m = (0, 0, p_m)$ . (b) Description of the excitation part of the protocol. We illuminate transversally the chain with a field whose spatial profile  $\Omega_n$  and frequency  $\omega_L$  are adjusted to excite the most superradiant singly-excited eigenmode  $|\psi_{\xi=N}^{(1)}\rangle$ . (c) Description of the transfer part of the scheme. We use a far off resonant electric field to create a detuning pattern whose sign can vary from an atom to its neighbour. (d) Representation of a V-shaped transition of an atom. The application of a far off resonant electric field  $\Omega_S$  with respect to the  $|g\rangle - |s\rangle$  transition allows to manipulate the detuning of the  $|g\rangle - |e\rangle$  transition with a spatial resolution given by  $\lambda_S$  potentially smaller than  $\lambda_{eg}$ . In the case of Dysprosium,  $\lambda_{eg} = 741\text{nm}$  and  $\lambda_S = 421\text{nm}$ .

total length larger than the wavelength to enable directivity and with a spacing smaller than half a wavelength to enhance interactions as represented in Fig. 1(a). It is composed of  $N$  three-level atoms ( $|g\rangle, |e\rangle, |s\rangle$ ) located at positions  $\mathbf{r}_m = (0, 0, ma)$ . The frequency of the  $|g\rangle - |e\rangle$  transition is given by  $\omega_{eg} = 2\pi c/\lambda_{eg}$  and its polarization is considered linear and parallel to the chain. A second transition depicted in Fig. 1(d) exists between  $|g\rangle$  and  $|s\rangle$  with a transition frequency  $\omega_S = 2\pi/\lambda_S$ . The role of this transition is dual. First, it enables the optical trapping of the atoms with a nearest neighbor distance  $a < \lambda_{eg}/2$  sufficiently small for subradiant modes to emerge. Second, it enables the realization of arbitrary detuning patterns [49] between the different atoms. It is a key point since the method we follow to manipulate collective states [45, 46] necessitate the realization of the so-called staggered pattern for which the local detuning of atom  $n$  changes sign from site to site:  $\Delta_n = (-1)^n \Delta$ . As a concrete example, we work with a conservative value of  $a/\lambda_{eg} = 0.35 < 0.5$  sufficiently small to create arbitrary PVD patterns and manipulate the subradiant modes that emerge in the atomic chain [45, 46]. This can be realized experimentally by loading an accordian lattice from an optical tweezer array [50].

### III. THEORETICAL MODEL

We now introduce the model used to describe the light chain interaction. We use the Born and Markov approximation [51, 52] to integrate out the photonic degrees of

freedom from the full atom-light system. This results in an interacting and open spin model, describing the dynamics of the atomic density matrix  $\rho$  with the Master equation (M.E):

$$\dot{\rho} = -i [\mathcal{H}\rho - \rho\mathcal{H}^\dagger] + \sum_{m,n} \Gamma_{m,n} \sigma_{eg}^m \rho \sigma_{ge}^n. \quad (1)$$

In this expression  $\mathcal{H} = \mathcal{H}_{\text{eff}} + \mathcal{H}_F + \mathcal{H}_S$  is the total Hamiltonian that includes : i) the effective Hamiltonian between the atoms  $\mathcal{H}_{\text{eff}}$  from which collective subradiant and superradiant modes emerge, ii) the interacting Hamiltonian between the atoms and the excitation field  $\mathcal{H}_F$  and iii) the interacting Hamiltonian induced by a detuning pattern  $\mathcal{H}_S$ . Both the population recycling term  $\Gamma_{m,n} = 2\mu_0\omega_0^2 \text{Im} [\mathbf{p}_n^* \overline{\mathbf{G}}(\mathbf{r}_n, \mathbf{r}_m, \omega_0) \mathbf{p}_m]$  and the effective Hamiltonian  $\mathcal{H}_{\text{eff}} = -\mu_0\omega_0^2 \sum_{m,n=1}^N \mathbf{p}_n^* \overline{\mathbf{G}}(\mathbf{r}_n, \mathbf{r}_m, \omega_0) \mathbf{p}_m \sigma_{eg}^m \sigma_{ge}^n$  depend on the free space dyadic electromagnetic Green's function  $\overline{\mathbf{G}}$ , the vacuum permeability  $\mu_0$ , the dipole of atom  $m$ :  $\mathbf{p}_m$ , and  $\sigma_{\alpha\beta} = |\alpha\rangle\langle\beta|$  with  $\{\alpha, \beta\} \in \{g, e\}$ . We model the excitation of the atoms with an intense coherent pulse using:  $\mathcal{H}_F = -\Delta_0(t) \sum_{n=1}^N \sigma_{ee}^n - \sum_n (\Omega_n(t) \sigma_{eg}^n + H.c)$ , with  $\Delta_0 = \omega_L - \omega_{eg}$  the detuning between the laser and atomic frequencies and  $\Omega_n$  the Rabi frequency of atom  $n$ . We represent the application of the PVD using  $\mathcal{H}_S = - \sum_{n=1}^N \Delta_n(t) \sigma_{ee}^n$ , with  $\Delta_n$  the local detuning of atom  $n$ . When needed, we can turn off the excitation and/or the detuning pattern setting  $\mathcal{H}_F$  and/or  $\mathcal{H}_S$  to 0 in Eq. (1).

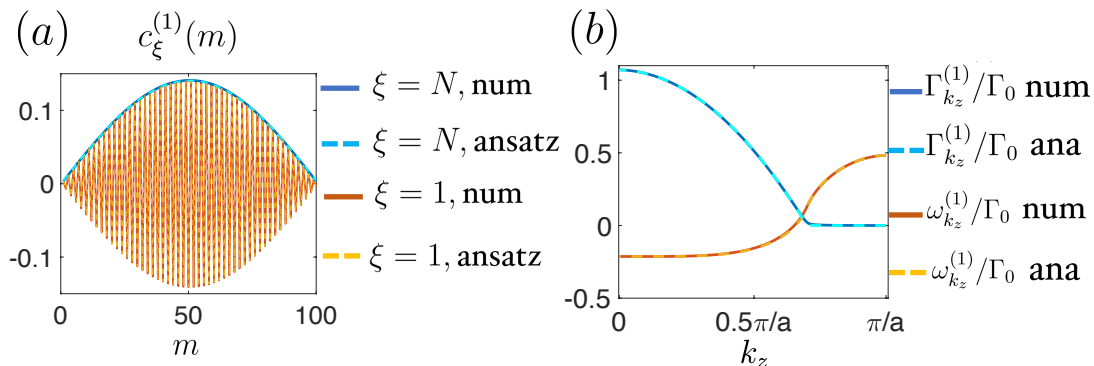


FIG. 2. a) Projection of  $|\psi_\xi^{(1)}\rangle = \sum_{m=1}^N c_\xi^{(1)}(m)|e_m\rangle$  on the physical basis of a chain composed of  $N = 100$  atoms, for both the most superradiant ( $\xi = N$  in blue) and subradiant singly-excited modes ( $\xi = 1$  in red). We compare with the expression given by the singly-excited ansatz  $|\psi_\xi^{\text{ans}}\rangle = \sqrt{\frac{2}{N+1}} \sum_{m=1}^N \sin\left(\frac{[N+1-\xi]m\pi}{N+1}\right)|e_m\rangle$  in dashed. b) Numerical evaluation of  $\omega_{k_z}^{(1)}/\Gamma_0$  (solid red) and  $\Gamma_{k_z}^{(1)}/\Gamma_0$  (solid blue) together with their analytical expression given in Eq. A1 and Eq. A2. The parameters are  $N = 100$  and  $a = 0.35\lambda_{eg}$  and the atomic polarization is linear and parallel to the chain.

### A. Spectral properties of singly and doubly-excited states.

To simplify the analysis of Eq. (1), we sort the eigenstates of  $\mathcal{H}_{\text{eff}}$  into different manifolds with a given number of excitations  $n_{\text{exc}} = (1, 2, \dots, N)$  and use the superscript  $(\dots)^{(n_{\text{exc}})}$  to label a given manifold. If for some specific reason,  $n_{\text{exc}} \leq n_{\text{max}}$  during the full dynamics, we truncate the Hilbert space to the populated manifolds only. Here, most of the results are presented with a numerical truncation of the Hilbert space to  $n_{\text{exc}} \leq 2$ . This both reduces the computation time and simplifies the analysis to the first two manifolds that we briefly describe below.

The diagonalization of  $\mathcal{H}_{\text{eff}}$  in the first manifold results in  $N$  eigenvectors  $|\psi_\xi^{(1)}\rangle = \sum_{m=1}^N c_\xi^{(1)}(m)|e_m\rangle$  such that  $\mathcal{H}_{\text{eff}}|\psi_\xi^{(1)}\rangle = (\omega_\xi^{(1)} - i\Gamma_\xi^{(1)}/2)|\psi_\xi^{(1)}\rangle$  where  $\omega_\xi^{(1)}$  represents the shift in energy of  $|\psi_\xi^{(1)}\rangle$  with respect to  $\omega_{eg}$  and  $\Gamma_\xi^{(1)}$  its decay rate. In order to differentiate easily the subradiant from the superradiant eigenmodes, we sort them from smallest to largest decay rate and label them with an integer denoted  $\xi$ . For example,  $|\psi_{\xi=1}^{(1)}\rangle$  is the most subradiant mode of the chain while  $|\psi_{\xi=N}^{(1)}\rangle$  is the most superradiant. In Fig. 2(a), we plot the amplitude of  $|\psi_\xi^{(1)}\rangle$  on each atom for both the most superradiant ( $\xi = N$ ) and subradiant singly-excited modes ( $\xi = 1$ ). We see that the singly-excited eigenmodes of an ordered chain are spin waves, well represented by the ansatz:  $|\psi_\xi^{\text{ans}}\rangle = \sqrt{\frac{2}{N+1}} \sum_{m=1}^N \sin\left(\frac{[N+1-\xi]m\pi}{N+1}\right)|e_m\rangle$  [26, 53]. Qualitatively, the most subradiant mode corresponds to a  $\pi$  phase difference between nearest neighbors whereas the superradiant mode corresponds to a uniform phase across the chain. In Fig. 2(b), we compute the decay rate and the frequency shift of each eigenmode and plot them as a function of  $k_z(\xi) = \frac{\pi(N+1-\xi)}{a(N+1)}$ . We observe strong

variations of the collective properties as a function of  $k_z$ , in perfect agreement with the analytical expressions given in appendix A. In particular, Fig. 2(b) clarifies the physics of super and subradiance: spin waves with a wave vector along the chain larger than  $\omega_{eg}/c$  cannot couple to electromagnetic waves in vacuum and are strongly subradiant. On the opposite, superradiant modes are associated with small values of  $k_z < \omega_{eg}/c$  [54–56].

We now turn to the excited manifolds and consider states with two excitations. Due to the atomic non-linearity, highly excited states are in general entangled, and very different from singly-excited ones [57–62]. Yet, in the specific case of a 1D ordered atomic chain composed of  $N \gg 1$  atoms, the  $N(N-1)/2$  doubly-excited states can be built as an anti-symmetric product of singly-excited spin waves [53, 56]. More precisely, we represent each doubly-excited state using the fermionic ansatz [53]:  $|\psi_{(\xi_1, \xi_2)}^{\text{ans}}\rangle = \sum_{m < n} [c_{\xi_1}^{(1)}(m)c_{\xi_2}^{(1)}(n) - c_{\xi_2}^{(1)}(m)c_{\xi_1}^{(1)}(n)] \sigma_{eg}^m \sigma_{eg}^n |g\rangle$ . In this expression, we used  $\xi^{(2)} = (\xi_1, \xi_2)$  to label this state and note that it is identical to the state labeled with  $(\xi_2, \xi_1)$  up to a minus sign. The consequence of the fermionic ansatz is that each doubly-excited state behaves like a doubly-excited spin wave, whose collective properties are well approximated by the sum of its single photon components:  $\Gamma_{(\xi_1, \xi_2)}^{(2)} \sim \Gamma_{\xi_1}^{(1)} + \Gamma_{\xi_2}^{(1)}$  and  $\omega_{(\xi_1, \xi_2)}^{(2)} \sim \omega_{\xi_1}^{(1)} + \omega_{\xi_2}^{(1)}$ . Let us conclude this section highlighting that the entanglement contained in the atomic degrees of freedom of a highly-excited state is an interesting resource whose extraction remains elusive for now [59, 60, 63–67]. A protocol, that permits the transfer of this entanglement to the emitted photons at a given time, and in a given direction would be key for quantum technologies.

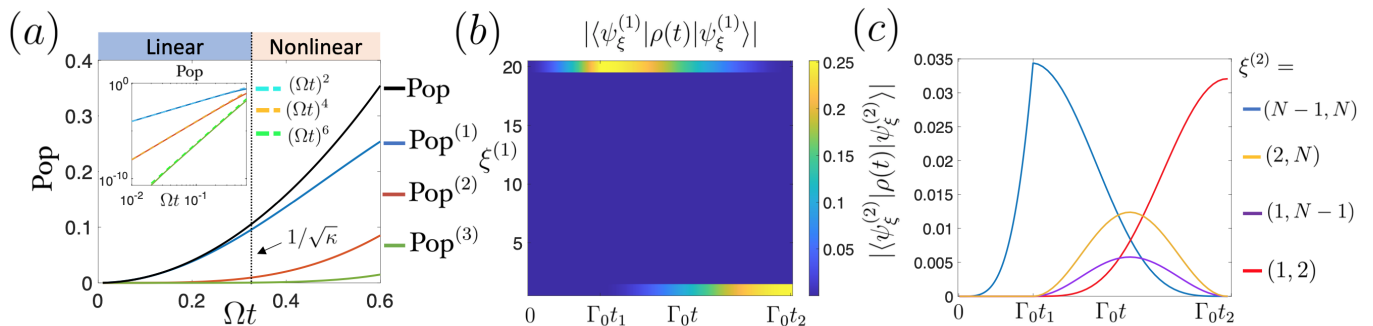


FIG. 3. a) Atomic population as a function of time during the illumination of the atomic system. The incident monochromatic field is adjusted spatially and spectrally to couple the ground state of the atomic system to the most superradiant singly-excited eigenmode. When  $\Omega t < 1$ , the population in each manifold (indicated by different colors) varies like  $(\Omega t)^{2n_{\text{exc}}}$ . The dotted vertical line represents the boundary between the linear and the nonlinear regime that depends on the ratio  $\kappa = \Gamma_{\xi=(1,2)}^{(2)}/\Gamma_{\xi=1}^{(1)}$  as discussed in appendix D. b) Projection of the density matrix onto each singly-excited eigenmodes during the first two steps of the protocol as a function of  $\Gamma_0 t$ . The illumination stops at  $t_1 = 0.6/\Omega$  and the transfer at  $t_2 = t_1 + \pi/(2\Delta)$ . c) Projection of the density matrix onto the four doubly-excited eigenmodes that dominates the doubly-excited population (indicated by different colors) during the first two steps of the protocol. Their label  $\xi^{(2)}$  is indicated in the caption. The numerical parameters are  $N = 20$ ,  $a = 0.35\lambda_{eg}$ , the atomic polarization is along the chain and the M.E equation has been truncated to 3 excitations in (a) and 2 in (b,c).  $\Omega = 100\Gamma_0$  and  $\Delta = 100\Gamma_0$  in (b,c).

#### IV. DESCRIPTION OF THE PROTOCOL

We detail below the different steps of the protocol.

##### A. Exciting the most superradiant mode.

We start by illuminating transversally the atomic system from the far field with a strong ( $\Omega \gg \Gamma_{\xi=N}^{(1)}$ ) and monochromatic laser field resonant with the most superradiant singly-excited eigenmode:  $\omega_L = \omega_{eg} + \omega_{\xi=N}^{(1)}$ . The spatial profile of the incident field:  $\Omega_n = \Omega \times \langle e_n | \psi_{\xi=N}^{(1)} \rangle$  is adjusted to couple preferentially the ground state to  $|\psi_{\xi=N}^{(1)}\rangle$ . This can be realized experimentally with state of the art SLM technologies. In Fig. 3(a) we study the populations in the first three manifolds when evolved with  $\mathcal{H} = \mathcal{H}_{\text{eff}} + \mathcal{H}_F$  for  $\Omega t < 1$ . We see in the insert that the population with  $n_{\text{exc}}$  excitations denoted  $\text{Pop}^{(n_{\text{exc}})}$  varies like  $(\Omega t)^{2n_{\text{exc}}}$ . As a consequence, the single photon population dominates when  $\Omega t \ll 1$ . This is the so-called linear regime studied in [45, 46] that neglects the inherent nonlinearity of atoms. In this work, we illuminate the system for longer times and reach a regime where both  $\text{Pop}^{(1)}$  and  $\text{Pop}^{(2)}$  contribute to the dynamics (while keeping  $\text{Pop}^{(3)} \ll 1$  for the sake of computation time). In this nonlinear regime, our protocol benefits both from the increase of the total population in the chain, and from the possibility to harness the entanglement of doubly-excited states. Moreover, the wavefront shaping of the incident beam proposed in this work simplifies the dynamics lowering the number of populated eigenmodes. Indeed, we plot in Fig. 3(b) the projection of the density matrix onto

each singly-excited eigenmode and observe that  $\text{Pop}^{(1)}$  is fully carried by the superradiant state  $|\psi_{\xi=N}^{(1)}\rangle$  during the illumination:  $\Gamma_0 t < \Gamma_0 t_1$ . In the second manifold, we observed numerically that the fermionic combination of the two most superradiant states  $|\psi_{\xi=(N-1,N)}^{(2)}\rangle$  largely dominates and contributes to  $\sim 70\%$  of  $\text{Pop}^{(2)}$  (see appendix C for an analytical justification).

##### B. Transfer to the most subradiant modes.

After an illumination time  $t_1$ , we stop the driving field and turn on the PVD:  $\mathcal{H} = \mathcal{H}_{\text{eff}} + \mathcal{H}_S$ . Since the eigenmodes of  $\mathcal{H}_{\text{eff}}$  are different from the eigenmodes of the total hamiltonian  $\mathcal{H}$ , the application of the PVD induces a transfer of population between the different  $|\psi_{\xi}^{(1)}\rangle$ . In the specific case of the staggered pattern:  $\Delta_n = (-1)^n \Delta$ , the matrix representation of  $\mathcal{H}_S$  in the singly-excited state basis of  $\mathcal{H}_{\text{eff}}$  is perfectly anti-diagonal [see Fig. 7(a)]. This means that the application of this PVD induces a one-to-one coupling between  $|\psi_{\xi}^{(1)}\rangle$  and  $|\psi_{N+1-\xi}^{(1)}\rangle$  [46]. More precisely, in the reduced basis built with  $\{|\psi_{\xi}^{(1)}\rangle, |\psi_{N+1-\xi}^{(1)}\rangle\}$  the coupling matrix writes:

$$\mathcal{H}_S = \begin{pmatrix} 0 & \Delta \\ \Delta & 0 \end{pmatrix}. \quad (2)$$

In Fig. 3(b), we plot the projection of the density matrix onto each singly-excited eigenmode as a function of time during the first two steps of the protocol. At the beginning of the transfer ( $t = t_1$ ),  $\text{Pop}^{(1)}$  is carried by  $|\psi_{\xi=N}^{(1)}\rangle$ . From  $t_1$  to  $t_2$ , we apply  $\mathcal{H}_S$  and observe a per-

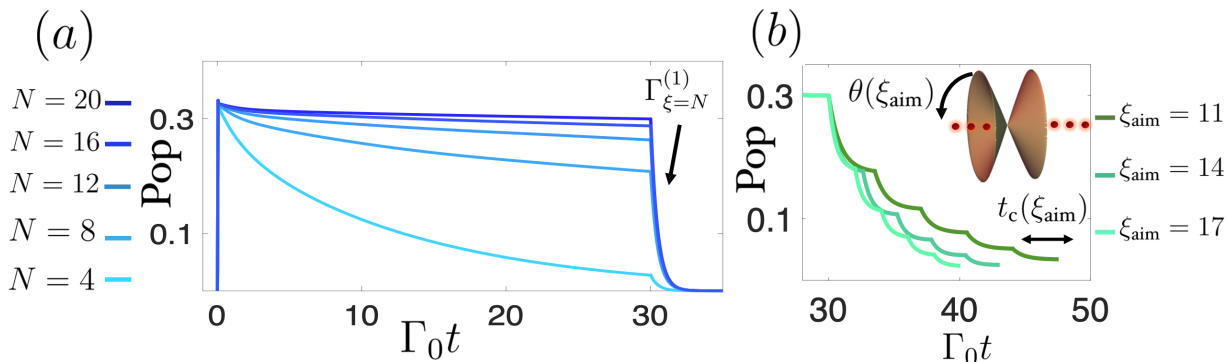


FIG. 4. a) Population in the chain as a function of time during the protocol for different  $N$  (indicated by different colors) and with  $\Omega t_1 = 0.6$ . (b) Emission step of the protocol with a control of the emitted mode  $\xi_{\text{aim}}$ . The emission process is split in  $N_c \sim 5$  cycles of duration  $t_c(\xi_{\text{aim}}) \sim 2/\Gamma_{\xi_{\text{aim}}}^{(1)}$ . As represented in insert, each mode emits in a cone of angle  $\theta(\xi_{\text{aim}})$  with respect to the atomic chain. The parameters are:  $a/\lambda_{eg} = 0.35$ ,  $N = 20$  and the polarization is linear and parallel to the chain. The M.E equation is numerically truncated to  $n_{\text{exc}} \leq 2$ .

fect transfer of the population to the most subradiant eigenmode  $|\psi_{\xi=1}^{(1)}\rangle$ . In the limit of a strong detuning:  $\Delta \gg |\omega_{\xi=N}^{(1)}|$  we can show that this transfer can be realized in a time  $t_t = t_2 - t_1 = \pi/(2\Delta) \ll 1/\Gamma_{\xi=N}^{(1)}$  small enough to neglect radiative loss.

Let us now push the analysis of the transfer to the two-photon population in the nonlinear regime. In this case, the coupling matrix in the complete doubly-excited state basis is harder to interpret visually. However, for a given initial state labeled with  $\xi^{(2)} = (\xi_1, \xi_2)$ , the evolution happens in a space of dimension 4 expressed in terms of the labels  $\xi^{(2)}$  for simplicity:  $\{(\xi_1, \xi_2), (N+1-\xi_1, \xi_2), (\xi_1, N+1-\xi_2), (N+1-\xi_1, N+1-\xi_2)\}$ . In this reduced basis, the transfer matrix has the form:

$$\mathcal{H}_S = \begin{pmatrix} 0 & -\Delta & \Delta & 0 \\ -\Delta & 0 & 0 & \Delta \\ \Delta & 0 & 0 & -\Delta \\ 0 & \Delta & -\Delta & 0 \end{pmatrix}. \quad (3)$$

Since 70% of the doubly-excited population is contained into the most superradiant doubly-excited state  $\xi^{(2)} = (N-1, N)$  at the beginning of the transfer, we can restrict the discussion to the evolution of this specific eigenmode. The application of the staggered pattern  $\mathcal{H}_S$  first couples equally the most superradiant doubly-excited state to  $\xi^{(2)} = (1, N-1)$  and  $\xi^{(2)} = (2, N)$ . We note that these states are built with the anti-symmetric product of one super and one subradiant singly-excited eigenstates and could be used for the heralded creation of subradiant states. Those states are in turn coupled to  $\xi^{(2)} = (1, 2)$  which is the most subradiant doubly-excited state. In order to illustrate this discussion, we plot in Fig. 3(c) the projection of the density matrix onto those four doubly-excited states. Note that there is a factor of two between the projection of the density matrix onto a doubly-excited state and the atomic population that it induces as we deal with doubly-excited states. At the beginning

of the transfer, we see in Fig. 3(c) that the projection of the density matrix is maximal onto the most superradiant doubly-excited state  $|\psi_{\xi=(N-1, N)}^{(2)}\rangle$ . It is then efficiently transferred to  $|\psi_{\xi=(1, 2)}^{(2)}\rangle$  in the exact same time  $t_t = \pi/(2\Delta)$  than derived for singly-excited states.

The application of the staggered pattern thus permits the coherent manipulation of doubly-excited states by switching their singly-excited components from superradiant to subradiant forms and vice-versa. We believe that the same phenomenon happens for larger excitation number ( $n_{\text{exc}} > 2$ ) as soon as the generalization of the fermionic ansatz is valid. This work thus enlarges the coherent control of collective states using the staggered pattern [45, 46] to higher manifolds.

### C. Storage.

After a transfer time  $t_t = \pi/(2\Delta)$ , we turn off  $\mathcal{H}_S$  and let the system evolve freely for sufficiently long times such that the loss term in Eq. (1) plays a role in the dynamics. In Fig. 4(a), we plot the total population in the chain during the complete protocol for various  $N$  indicated by different colors. Due to the open character of the system, we observe a decrease of the atomic population during the storage ( $t_2 < t < 30\Gamma_0$ ), which reveals that photons are emitted by the atomic chain. Importantly, we observe that the storage of the atomic population increases with the system size  $N$ .

To discuss this first observation, we simplify the problem neglecting the  $\sim 30\%$  of  $\text{Pop}^{(2)}$  not contained into  $|\psi_{\xi=(1, 2)}^{(2)}\rangle$  and approximate the state of the system at the end of the transfer by the pure state  $|\psi(t_2)\rangle \propto (\Omega t_1)|\psi_{\xi=1}^{(1)}\rangle + \frac{(\Omega t_1)^2}{\sqrt{2}}|\psi_{\xi=(1, 2)}^{(2)}\rangle$ . Then, we follow [68] and use a rate model (R.M) described in appendices B and D that simplifies the analysis. Doing so, we restrict the

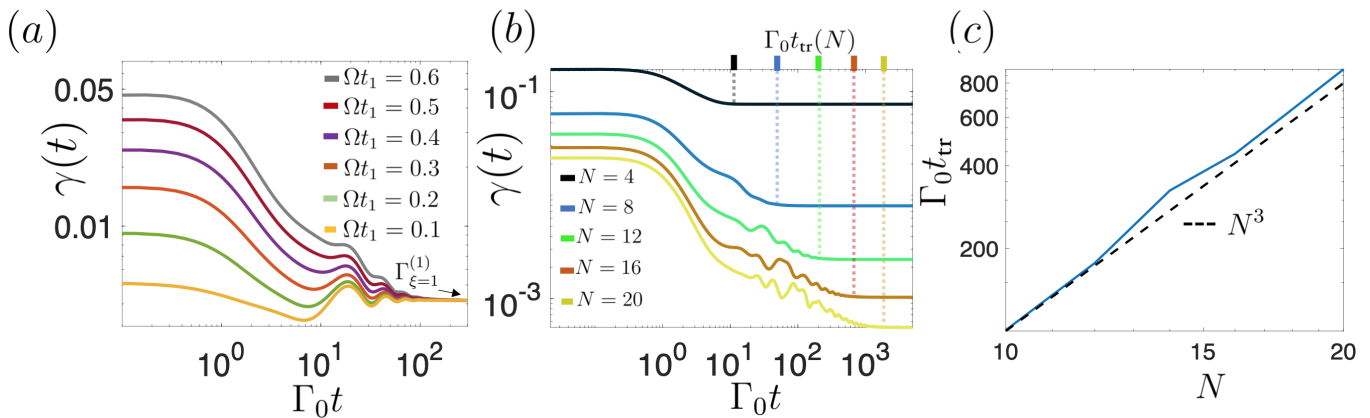


FIG. 5. a) Numerical calculation of  $\gamma(t)$  during the storage for various  $\Omega t_1$  for a fixed  $N = 10$ . We highlight with a black arrow the long time value of  $\gamma(t) = \Gamma_{\xi=1}^{(1)}$ . In (b), we fix  $\Omega t_1 = 0.6$  and vary  $N$ . We project on top of the figure the value of the transition time between the "short" and the "long" time behavior:  $\Gamma_0 t_{\text{tr}}(N)$ . In (c) we plot  $\Gamma_0 t_{\text{tr}}$  extracted from the simulations as a function of  $N$  and compare it with a  $N^3$  scaling. The parameters are:  $a/\lambda_{\text{eg}} = 0.35$ ,  $n_{\text{exc}} \leq 2$ ,  $N = 10$  [in (a)] and  $\Omega t_1 = 0.6$  in (b,c). The atomic polarization is linear and parallel to the chain. In (a,b) the origin of time is taken at the beginning of the storage.

the dynamics under free evolution in the presence of loss to a subspace built by the *last two survivors*  $|\psi_{\xi=1}^{(1)}\rangle$  and  $|\psi_{\xi=(1,2)}^{(2)}\rangle$ . This simplification leads to the following expression for the total atomic population:

$$\text{Pop}(t) = (\Omega t_1)^2 e^{-\Gamma_{\xi=1}^{(1)} t} + (\Omega t_1)^4 e^{-\Gamma_{\xi=(1,2)}^{(2)} t} \quad (4)$$

where the first term of the right hand side represents  $\text{Pop}^{(1)}$  and the second term  $\text{Pop}^{(2)}$ . Since  $|\psi_{\xi=(1)}^{(1)}\rangle$  and  $|\psi_{\xi=(1,2)}^{(2)}\rangle$  are subradiant, both  $\Gamma_{\xi=1}^{(1)}$  and  $\Gamma_{\xi=(1,2)}^{(2)}$  decrease as  $1/N^3$ . Injecting those scalings into Eq. (4) directly permits to recover the improvement of the storage of the total population when the system size increases observed numerically in Fig. 4(a).

Next, we push the analysis further comparing the rate of emission of photons coming from singly and doubly-excited states. To do so we study the instantaneous decay rate [69]:

$$\gamma(t) = -\text{Pop}'/\text{Pop} \quad (5)$$

during the storage, for various  $N$  and different values of  $\Omega t_1$ . In Fig. 5(a) we plot the numerical value of  $\gamma(t)$  for  $N = 10$  and  $\Omega t_1$  varying from 0.1 to 0.6. We see that whatever the value of  $\Omega t_1$ ,  $\gamma(t)$  converges at "long" times towards a plateau whose value is given by  $\Gamma_{\xi=1}^{(1)}$ . This means that the emission of photons at "long" times is dominated by single photons radiated by the most sub-radiant singly-excited state.

Next we turn to the study of the "short" time regime of  $\gamma(t)$  observed in Fig. 5(a) where  $\gamma(t)$  varies with  $\Omega t_1$ . To understand this point, we inject Eq. 4 into Eq. 5 and obtain a simplified expression of  $\gamma(t)$  predicted by the

R.M. It writes:

$$\gamma(t) = \Gamma_{\xi=1}^{(1)} \frac{e^{-\Gamma_{\xi=1}^{(1)} t} + \kappa (\Omega t_1)^2 e^{-\Gamma_{\xi=(1,2)}^{(2)} t}}{e^{-\Gamma_{\xi=1}^{(1)} t} + (\Omega t_1)^2 e^{-\Gamma_{\xi=(1,2)}^{(2)} t}}, \quad (6)$$

with  $\kappa > 1$  the proportionality factor between  $\Gamma_{\xi=1}^{(1)} = \alpha_1 N^{-3}$  and  $\Gamma_{\xi=(1,2)}^{(2)} = \kappa \alpha_1 N^{-3}$  which comes from the fermionic ansatz [53]. In Fig. 8(b), we compare Eq. (6) with the exact calculation of  $\gamma(t)$  using the M.E and observe that Eq. (6) slightly underestimates the instantaneous decay at short times. This comes from the neglect of the  $\sim 30\%$  of  $\text{Pop}^{(2)}$  not contained into  $|\psi_{\xi=(1,2)}^{(2)}\rangle$ . Nonetheless the R.M still captures the increase of  $\gamma(0)$  when  $\Omega t_1$  increases, and shows that this effect comes from the competition between the singly and doubly-excited decay. More importantly, we observe in Fig. 8(b) that Eq. (6) properly captures the dynamical transition between the short and long time regimes of  $\gamma(t)$ . Hence the R.M permits to set the boundary between a short time regime where the emission is dominated by  $\text{Pop}^{(2)}$  and a long time regime where it is dominated by  $\text{Pop}^{(1)}$ . To do so, we introduce the transition time  $t_{\text{tr}}$  such as the time needed for  $\gamma(t)$  to converge towards  $\Gamma_{\xi=1}^{(1)}$ . We obtain its analytical expression using Eq. 6 using the condition that the weight of the single and two-photon decay should be equal at this specific time. We obtain:

$$t_{\text{tr}} = \frac{\log(\kappa (\Omega t_1)^2)}{(\kappa - 1) \alpha_1} N^3 \quad (7)$$

with  $\kappa = \Gamma_{\xi=(1,2)}^{(2)}/\Gamma_{\xi=(1)}^{(1)}$  the ratio between the two decay rates almost constant to a value around 9 for large systems (see Appendix D).

In Fig. 5(b), we fix  $\Omega t_1 = 0.6$ , vary  $N$  from 4 to 20 and extract the numerical value of  $t_{\text{tr}}$  that we project on top of the figure for the sake of clarity. In Fig. 5(c), we plot the extracted value of  $t_{\text{tr}}$  as a function of the system size and confirm numerically the variation of  $t_{\text{tr}} \sim N^3$  predicted by Eq. 7. This scaling shows that doubly-excited states dominate the emission for a time that strongly increases with the system size. Besides, Eq. 7 tells us that  $t_{\text{tr}}$  only exists if  $\Omega t_1 > \kappa^{-1/2}$  (due to the log). The condition  $\Omega t_1 > \kappa^{-1/2}$  depicted in Fig. 3(a) thus sets the boundary between the linear and the nonlinear regime (in terms of illumination strength) to  $\Omega t_1 = 1/\sqrt{\kappa} \sim 0.3$ . This order of magnitude is confirmed numerically in Fig. 5(a) in which we can estimate the minimum value of  $\Omega t_1$  such that  $\text{Pop}^{(2)}$  dominates the decay at short times to  $\sim 0.2$ .

To conclude this section, we proposed a simplified model of the dynamics during the storage in order to compute the minimal value of the illumination strength  $\Omega t_1$  needed to access the onset of the non-linear regime. In this regime, we showed that the two-photon population dominates the emission of photons for a duration that strongly increases with the system size.

#### D. Emission.

After a sufficiently long storage time such that the two-photon population is completely negligible, the remaining population is fully carried by the most subradiant singly-excited state  $|\psi_{\xi=1}^{(1)}\rangle$ . On demand, one can turn on the PVD, transfer back the population to the most superradiant singly-excited mode in a time  $t_t = \pi/(2\Delta)$ , and then let evolve the state with  $\mathcal{H}_{\text{eff}}$ . Doing so, the atomic population decays at a rate  $\Gamma_{\xi=N}^{(1)}$ , as observed in Fig. 4(a). In order to control the emission rate:  $\Gamma_{\xi_{\text{aim}}}^{(1)}$ , the frequency  $\omega_{\xi_{\text{aim}}}^{(1)}$  and the radiation pattern of the emitted single-photon, we introduce a new sinusoidal PVD:

$$\Delta_n(t) = \Delta \sin\left(\frac{n\xi_{\text{aim}}\pi}{N+1}\right) \quad (8)$$

that couples the most subradiant eigenmode  $|\psi_{\xi=1}^{(1)}\rangle$  to  $|\psi_{\xi_{\text{aim}}}^{(1)}\rangle$ . As observed in Fig. 7(c) this coupling is not perfectly one-to-one, and rather looks like a sinc function. In order to avoid second order coupling to subradiant states which would prevent the efficient emission of the photon, we split the emission procedure in  $N_c \sim 5$  cycles. Each cycle contains one transfer step using the sinusoidal PVD of duration  $t = \pi/(3\Delta)$  short enough for enabling first order coupling only, and one free evolution step of duration  $t = 2/\Gamma_{\xi_{\text{aim}}}^{(1)}$ . This method enables the efficient emission of the photon mostly through the mode indexed  $\xi_{\text{aim}}$  as shown in Fig. 4(b). We compute the radiation pattern of the atomic ensemble using:  $\mathbf{E}(\mathbf{r}) = \mu_0\omega_0^2 \sum_{n=1}^N \overline{\mathbf{G}}(\mathbf{r}, \mathbf{r}_n, \omega_0) \mathbf{p}_n \langle \sigma_{ge}^n \rangle$  with  $\langle \sigma_{ge}^n \rangle = \text{Tr}(\sigma_{ge}^n \rho)$

obtained from the resolution of eq. (1). The radiation pattern of one typical superradiant mode indexed with  $\xi_{\text{aim}} \neq N$  is given the inset of Fig. 4(b). For atoms linearly polarized along the chain, we see that the mode with label  $\xi_{\text{aim}}$  emits in a cone of angle  $\theta(\xi_{\text{aim}})$  that directly depends on  $k_z$ :  $\theta(\xi_{\text{aim}}) = \text{atan}(k_{\perp}/k_z)$ , with  $k_z = \frac{\pi(N+1-\xi_{\text{aim}})}{a(N+1)}$  and  $k_{\perp} = \sqrt{\omega_{eg}^2/c^2 - k_z^2}$ . Perfect retrieval of the emitted single-photon can thus be realized with two lenses of proper NA.

## V. CONCLUSION

In summary, we studied theoretically a protocol that enables on-demand absorption, storage, and re-emission of an incident field using subradiant and superradiant states of an atomic chain. The three-level nature of the atoms allows both their trapping and manipulation using light shifts with a resolution smaller than  $\lambda_{eg}$ . This permits the deterministic coupling to subradiant states, which are important resources for metrology [70, 71] or quantum computing [72, 73]. Valid beyond the linear regime, our theoretical analysis provides an intuitive picture of the dynamics in terms of singly and doubly-excited states. For the first time to our knowledge, we discuss the manipulation of multiply excited states using tailored PVDs combined with shaped incident fields. We envision in the future to study the efficient excitation of highly excited states in order to control the quantum correlations of light emitted by the array [63, 67]. Quantum metamaterials [74, 75], such as 2D arrays have already been shown to act as a subradiant mirrors [24, 27, 44] or proposed to construct lossless 1D atomic waveguides [53, 76]. Adjusting their many-body functionalities on demand, in a time shorter than the emission time is a largely unexplored avenue that would enlarge their potential as versatile light-matter interfaces.

## ACKNOWLEDGEMENTS

We acknowledge Ilan Shlesinger and Jean-Paul Hugonin for important discussions. A.B. and I.F-B acknowledge funding from the European Research Council (Grants. No. 101018511, ATARAXIA, 101039361, CORSAIR) and by the Agence National de la Recherche (ANR, project DEAR).

### Appendix A: Collective properties of singly-excited states

In this appendix, we remind the analytical expressions of  $\Gamma_{k_z}^{(1)}$  and  $\omega_{k_z}^{(1)}$  derived in the literature [26, 53] in order to understand the collective properties of the eigenmodes of the effective Hamiltonian.  $\Gamma_{k_z}^{(1)}$  can be expressed in terms of the reciprocal lattice vectors  $g_z$ , and writes (for

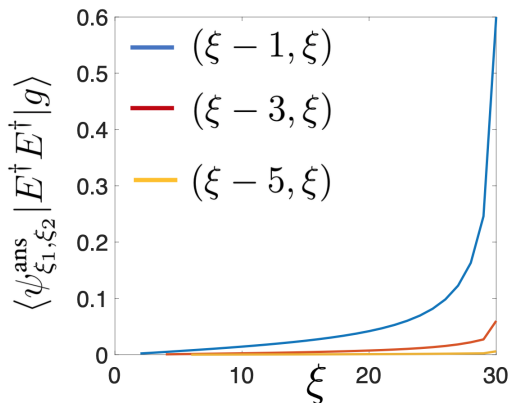


FIG. 6. Numerical calculation of  $\langle \psi_{\xi_1, \xi_2}^{\text{ans}} | E^\dagger E^\dagger | g \rangle / (\mathcal{N} \Omega^2)$  given Eq. (C2). We study three different types of doubly-excited states built with the anti-symmetric product of singly-excited eigenmodes with labels  $(\xi - 1, \xi)$  (blue),  $(\xi - 3, \xi)$  (red) and  $(\xi - 5, \xi)$  (yellow) as a function of  $\xi$ . The system size is  $N = 30$ ,  $\Omega = 1$ , and the eigenmodes have been computed with an atomic polarization parallel to the chain.

a linear atomic polarization along the chain):

$$\frac{\Gamma_{k_z}^{(1)}}{\Gamma_0} = \frac{3\pi}{2k_0 a} \sum_{|k_z + g_z| < k_0} \left( 1 - \frac{(k_z + g_z)^2}{k_0^2} \right). \quad (\text{A1})$$

The analytical expression of  $\omega_{k_z}^{(1)}$  can be obtained using the mathematical function  $\text{Li}_s(z) = \sum_{l=1}^{\infty} z^l e^{-s}$ ,  $Z_1 = e^{i(k_0 + k_z)a}$  and  $Z_2 = e^{i(k_0 - k_z)a}$ . It writes:

$$\frac{\omega_{k_z}^{(1)}}{\Gamma_0} = -\frac{3\pi}{2k_0^3 a^3} (\text{Li}_3(Z_1) + \text{Li}_3(Z_2) - ik_0 a [\text{Li}_2(Z_1) + \text{Li}_2(Z_2)]). \quad (\text{A2})$$

We stress here that those quantities depends on the atomic polarization. The numerical results presented in this work have been derived for a linear polarization along the chain. However, they can be easily extended to the same system with circular atomic polarization simply by adapting the exact value of the decay rates and the frequency shifts [26, 53]. For an atomic polarization linear and orthogonal to the chain (along  $x$  for instance), the link between  $\xi$  and  $k_z$  is more involved, but the physics of super and subradiance remains the same. Namely, spin waves with a wave vector along the chain larger than  $\omega_{eg}/c$  cannot couple to electromagnetic waves in vacuum and are strongly subradiant. On the opposite, superradiant modes are associated with small values of  $k_z < \omega_{eg}/c$ .

### Appendix B: Decay of the doubly-excited eigenmodes

In this appendix, we remind some properties of the most super and subradiant doubly-excited states useful

to understand the population dynamics during the protocol in the nonlinear regime. The most subradiant (respectively superradiant) doubly-excited eigenmode is built as a fermionic product of singly-excited states with indexes  $(\xi_1 = 1, \xi_2 = 2)$  [respectively  $(\xi_1 = N - 1, \xi_2 = N)$ ]. As a direct consequence, the most superradiant doubly-excited eigenmode mostly decays into the singly-excited states of indexes  $\xi_1 = N - 1$  and  $\xi_2 = N$  while the most subradiant decays into  $\xi_1 = 1$  and  $\xi_2 = 2$  [68]. The reduction of the number of states involved in the decay process enables the use of a simplified rate model involving only 3 different states:  $\{|\psi_{\xi_1}^{(1)}\rangle, |\psi_{\xi_2}^{(1)}\rangle, |\psi_{\xi}^{(2)}\rangle\}$ :

$$\begin{cases} dc_{\xi}^{(2)}/dt = -\Gamma_{\xi}^{(2)} c_{\xi}^{(2)} \\ dc_{\xi_1}^{(1)}/dt = -\Gamma_{\xi_1}^{(1)} c_{\xi_1}^{(1)} + \gamma_{\xi_1, \xi} c_{\xi}^{(2)} \\ dc_{\xi_2}^{(1)}/dt = -\Gamma_{\xi_2}^{(1)} c_{\xi_2}^{(1)} + \gamma_{\xi_2, \xi} c_{\xi}^{(2)} \end{cases} \quad (\text{B1})$$

with  $c_{\xi}^{(2)}$  the population of the doubly-excited mode,  $c_{\xi_1}^{(1)}$  and  $c_{\xi_2}^{(1)}$  the population of the singly-excited modes into which it decays. The decay rate from state  $|\psi_{\xi'}^{(2)}\rangle$  to state  $|\psi_{\xi}^{(1)}\rangle$  can be computed using  $\gamma_{\xi, \xi'} = \text{Tr}(|\psi_{\xi}^{(1)}\rangle \langle \psi_{\xi}^{(1)}| \mathcal{J} |\psi_{\xi'}^{(2)}\rangle \langle \psi_{\xi'}^{(2)}|)$ , with  $\mathcal{J} = \sum_{m, n} \Gamma_{m, n} \sigma_{eg}^m \rho \sigma_{ge}^n$  the recycling operator of the M.E given in Eq. (1) of the main text.

## Appendix C: Details of the steps of the protocol

### 1. Coupling with the field

We chose the field operator  $E^\dagger = \Omega \sum_i c_{\xi=N}^{(1)}(i) \sigma_{eg}^i$  in order to couple the ground state to  $|\psi_{\xi=N}^{(1)}\rangle$  efficiently. Indeed, one can check numerically or analytically that  $\langle \psi_{\xi}^{(1)} | E^\dagger | g \rangle = \Omega \delta(\xi - N)$ . However we do not know *a priori* which doubly-excited eigenstates are populated when the field operator is applied twice to the ground state and creates  $E^\dagger E^\dagger | g \rangle = \Omega^2 \sum_{i < j} c_{\xi=N}^{(1)}(i) c_{\xi=N}^{(1)}(j) \sigma_{eg}^i \sigma_{eg}^j | g \rangle$ . To identify this state, we take its dot product with every two-photon ansatz states:  $\langle \psi_{(\xi_1, \xi_2)}^{\text{ans}} | E^\dagger E^\dagger | g \rangle$  using:

$$\begin{aligned} |\psi_{(\xi_1, \xi_2)}^{\text{ans}}\rangle = \mathcal{N} \sum_{m < n} & \left[ c_{\xi_1}^{(1)}(m) c_{\xi_2}^{(1)}(n) - c_{\xi_2}^{(1)}(m) c_{\xi_1}^{(1)}(n) \right] \\ & \times \sigma_{eg}^m \sigma_{eg}^n | g \rangle, \end{aligned} \quad (\text{C1})$$

with  $\mathcal{N}$  a normalization factor and  $c_{\xi}^{(1)}(i) = \sqrt{\frac{2}{N+1}} \sin\left[\frac{(N+1-\xi)i\pi}{N+1}\right]$  the singly-excited eigenmode ansatz. This leads to a rather long expression:



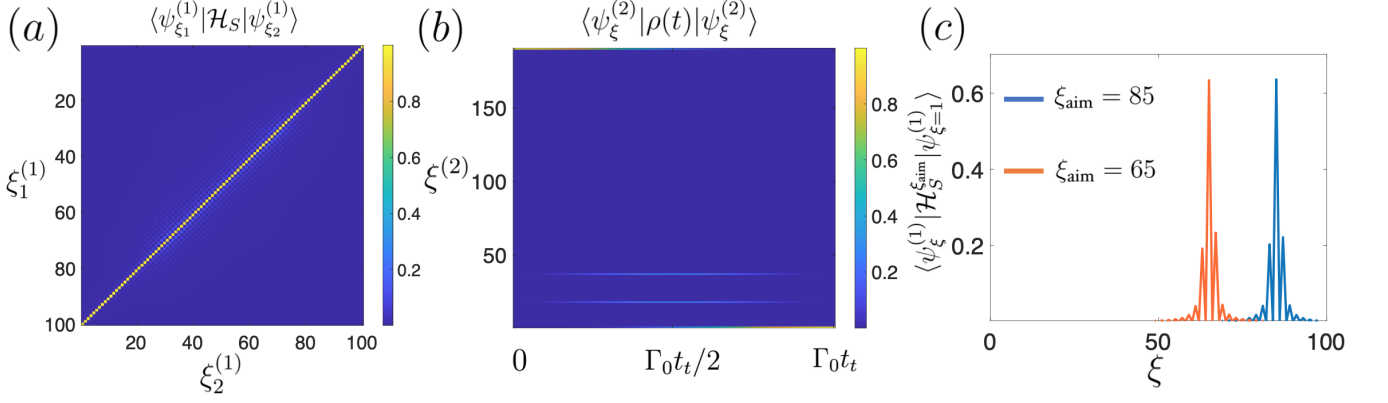


FIG. 7. a) Matrix element of  $\mathcal{H}_S$  (with a staggered pattern) in the basis built with the different eigenmodes  $|\psi_{\xi}^{(1)}\rangle$ . b) Projection of the time evolved density matrix onto the doubly-excited eigenmodes during the transfer with the most superradiant doubly-excited state. We observe that the two-photon population starts in  $\xi^{(2)} = \binom{N}{2} = 190$  before being split into two intermediate states  $\xi^{(2)} = N = 20$  and  $\xi^{(2)} = N + N - 1 = 39$  (half super and half subradiant) and terminates the transfer into  $\xi^{(2)} = 1$ . In this plot,  $\xi^{(2)}$  is not a 2D vector but a number that sorts the doubly-excited eigenmodes with respect to their decay rate. c) Coupling parameter between  $|\psi_{\xi=1}^{(1)}\rangle$  and  $|\psi_{\xi}^{(1)}\rangle$  induced by the sinusoidal PVD:  $\mathcal{H}_S^{\xi_{\text{aim}}}$  for  $\xi_{\text{aim}} = 65$  (red) and  $\xi_{\text{aim}} = 85$  (blue). The parameters are  $N = 100$ ,  $a = 0.35\lambda_{eg}$  and  $\Delta = \Gamma_0$  in (a,c). In (b) we considered  $N = 20$ ,  $a = 0.35\lambda_{eg}$  and  $\Delta = 100\Gamma_0$ . The atomic polarization is parallel to the chain.

$$\begin{aligned} \langle \psi_{\xi_1, \xi_2}^{\text{ans}} | E^\dagger E^\dagger | g \rangle &= \mathcal{N} \sum_{i < j} \frac{4\Omega^2}{(N+1)^2} \sin \left[ \frac{i\pi}{N+1} \right] \sin \left[ \frac{j\pi}{N+1} \right] \\ &\times \left[ \sin \left[ \frac{(N+1-\xi_1)i\pi}{N+1} \right] \sin \left[ \frac{(N+1-\xi_2)j\pi}{N+1} \right] \right. \\ &\left. - \sin \left[ \frac{(N+1-\xi_2)i\pi}{N+1} \right] \sin \left[ \frac{(N+1-\xi_1)j\pi}{N+1} \right] \right] \end{aligned} \quad (\text{C2})$$

that we evaluate numerically in Fig. 6. We show that, when applied two times on the ground state, the field preferentially couples to  $|\psi_{(\xi_1=N-1, \xi_2=N)}^{\text{ans}}\rangle$ : the most superradiant doubly-excited state. One should note that a part of the two-photon population is carried by other modes ( $\sim 30\%$  of the two-photon population observed numerically). This 30% of  $\text{Pop}^{(2)}$  is responsible for the discrepancy observed at short times in the evaluation of  $\gamma(t)$  using the R.M and the M.E observed in Fig. 8(b).

## 2. Modes transfer using PVD

In this subsection, we provide additional details about mode transfer using PVD. In Fig. 7(a) we represent  $|\langle \psi_{\xi_1}^{(1)} | \mathcal{H}_S | \psi_{\xi_2}^{(1)} \rangle|$  and observe an almost perfect anti-diagonal matrix. This means that, the evolution of an eigenmode with label  $\xi$  of  $\mathcal{H}_{\text{eff}}$  under the application of the staggered pattern happens in a space of dimension 2:  $\{|\psi_{\xi}^{(1)}\rangle, |\psi_{N+1-\xi}^{(1)}\rangle\}$ .

In the second manifold, we choose not to represent the matrix elements  $|\langle \psi_{\xi_1}^{(2)} | \mathcal{H}_S | \psi_{\xi_2}^{(2)} \rangle|$  as they are difficult to

interpret visually. Instead, we plot in Fig. 7(b) the projection of the density matrix onto each doubly-excited eigenmode during the transfer. In this plot,  $\xi^{(2)}$  is not a 2D vector but a number that sorts the doubly-excited eigenmodes with respect to their decay rate. The initial state is the most superradiant doubly-excited state associated with  $\xi^{(2)} = \binom{N}{2} = 190$  (for  $N = 20$  atoms). It is then equally transferred to the doubly-excited state of index  $\xi^{(2)} = N = 20$  (built with the product of  $|\psi_{\xi=1}^{(1)}\rangle$  and  $|\psi_{\xi=N}^{(1)}\rangle$ ) and the doubly-excited state of index  $\xi^{(2)} = N + (N - 1) = 39$  (built with the product of  $|\psi_{\xi=2}^{(1)}\rangle$  and  $|\psi_{\xi=N-1}^{(1)}\rangle$ ). Eventually, those two modes are coupled to the most subradiant doubly-excited state associated with  $\xi^{(2)} = 1$  (built with the product of  $|\psi_{\xi=1}^{(1)}\rangle$  and  $|\psi_{\xi=2}^{(1)}\rangle$ ).

At the end of the storage, we want to transfer back the singly-excited subradiant state into the superradiant mode of our choice. Thus, we use the following sinusoidal PVD:  $\mathcal{H}_S^{\xi_{\text{aim}}} = -\sum_{n=1}^N \Delta_n \sigma_{ee}^n$  with  $\Delta_n = \Delta \sin[n\xi_{\text{aim}}\pi/(N+1)]$ . This detuning pattern mostly couples the most subradiant mode ( $\xi = 1$ ) to the eigenstate with label  $\xi_{\text{aim}}$  as observed in Fig. 7(c). However, since the coupling is not one to one (it rather looks like a sinc function), the emission protocol should be split into  $N_c = 5$  cycles. Each cycle contains one transfer step using the sinusoidal PVD of duration  $t = \pi/(3\Delta)$  and one free evolution step of duration  $t = 2/\Gamma_{\xi_{\text{aim}}}^{(1)}$ . With this method, we can funnel most of the emission through the singly-excited eigenmode with label  $\xi_{\text{aim}}$  and avoid residual coupling to subradiant eigenmodes.

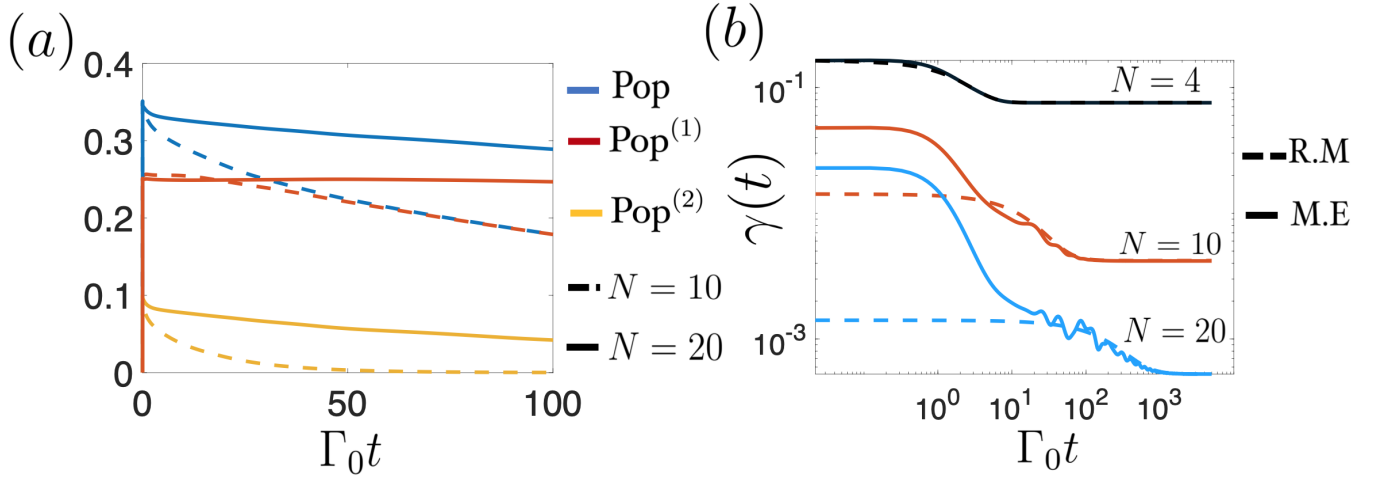


FIG. 8. a) Total population (blue), population in the first (red) and second (yellow) manifolds as a function of time for  $N = 10$  (dashed) and  $N = 20$  (solid lines) b) Numerical calculation  $\gamma(t)$  during the storage for various  $N$  and  $\Omega t_1 = 0.6$ . In solid lines we plot the results given by the M.E. and in dashed the results given by the R.M. The Hilbert space has been truncated to  $n_{\text{exc}} \leq 2$ , we considered atomic polarization linear and parallel to the chain, and an interatomic distance  $a/\lambda_{eg} = 0.35$ . In (b) the origin of time is taken at the beginning of the storage ( $t = t_2$ ).

#### Appendix D: Last two survivors approximation

In this section, we provide additional details about the analysis of the role of the two-photon population during the storage. As a first observation, we plot in Fig. 8(a) the total population (blue), the population of the single photon components (red) and two-photon components (yellow) for two different system sizes ( $N = 10$  in dashed and  $N = 20$  in solid lines) for  $\Omega t_1 = 0.6$ . We observe that both the single and the two-photon components are better stored as  $N$  increases and clearly observe that the two-photon population can not be neglected for "short" times.

In Fig. 8(b) we compare the value of  $\gamma(t)$  given by the R.M. and by the M.E. We observe a good agreement for both the long time value of  $\gamma(t)$  and  $t_{\text{tr}}$  as discussed in the main text. This shows that we can use the reduced set of states of the R.M:  $\{|\psi_{\xi=1}^{(1)}\rangle, |\psi_{\xi=2}^{(1)}\rangle, |\psi_{\xi=(1,2)}^{(2)}\rangle\}$  to compute the dynamics for  $t \geq t_{\text{tr}}$ . To do so, we express the total population during the storage in the reduced basis:

$$\text{Pop}(t) = c_{\xi=1}^{(1)}(t) + c_{\xi=2}^{(1)}(t) + 2c_{\xi=(1,2)}^{(2)}(t) \quad (\text{D1})$$

with  $c_{\xi=1}^{(1)}(t)$ ,  $c_{\xi=2}^{(1)}(t)$  and  $c_{\xi=(1,2)}^{(2)}(t)$  the population of the three modes involved. Their initial values at  $t = 0$  (beginning of the storage) depend on  $\Omega t_1$ :  $c_{\xi=1}^{(1)}(0) = (\Omega t_1)^2$ ,  $c_{\xi=2}^{(1)}(0) = 0$  and  $2c_{\xi=(1,2)}^{(2)}(0) \sim (\Omega t_1)^4$  and their dynamics can be solved numerically using eq. B1. In this specific study of the transition time  $t_{\text{tr}}$ ,  $c_{\xi=2}^{(1)}(t)$  plays a negligible role as both its population and decay rate are low. We thus reduce the analytical analysis to the *last two survivors*  $c_{\xi=1}^{(1)}(t)$  and  $c_{\xi=(1,2)}^{(2)}(t)$ , neglect the filling of

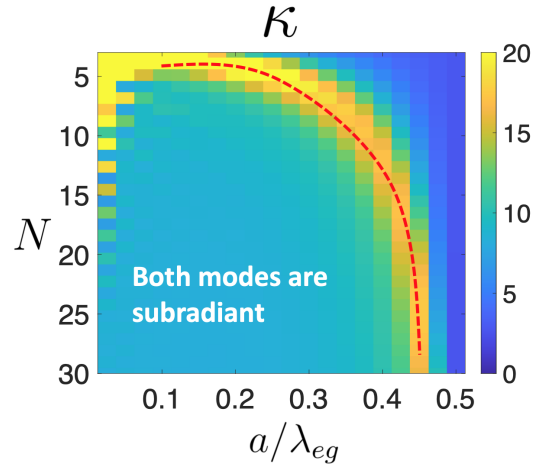


FIG. 9. a) Numerical calculation of  $\kappa = \Gamma_{\xi=(1,2)}^{(2)}/\Gamma_{\xi=1}^{(1)}$  as a function of  $N$  and  $a/\lambda_{eg}$ . In the regime where both modes are subradiant,  $\kappa$  is found to be almost constant and close to 9. In dashed red, we highlight the parameters for which the most subradiant doubly-excited state becomes superradiant (due to finite size effects) while the singly-excited one remains subradiant. This results in an increase of  $\kappa$ . Outside this domain, both modes are radiants. We considered atomic polarization linear and parallel to the chain.

$c_{\xi=1}^{(1)}(t)$  due to the decay of  $c_{\xi=(1,2)}^{(2)}(t)$  in order to obtain the simplified expression of the total population provided in Eq. 4. Equation 4 is written in terms of  $\Gamma_{\xi=1}^{(1)} = \alpha_1 N^{-3}$  and  $\Gamma_{\xi=(1,2)}^{(2)} = \kappa \alpha_1 N^{-3}$ , which are the decay rates of the most subradiant singly and doubly-excited states.  $\kappa$  represents the ratio between the two

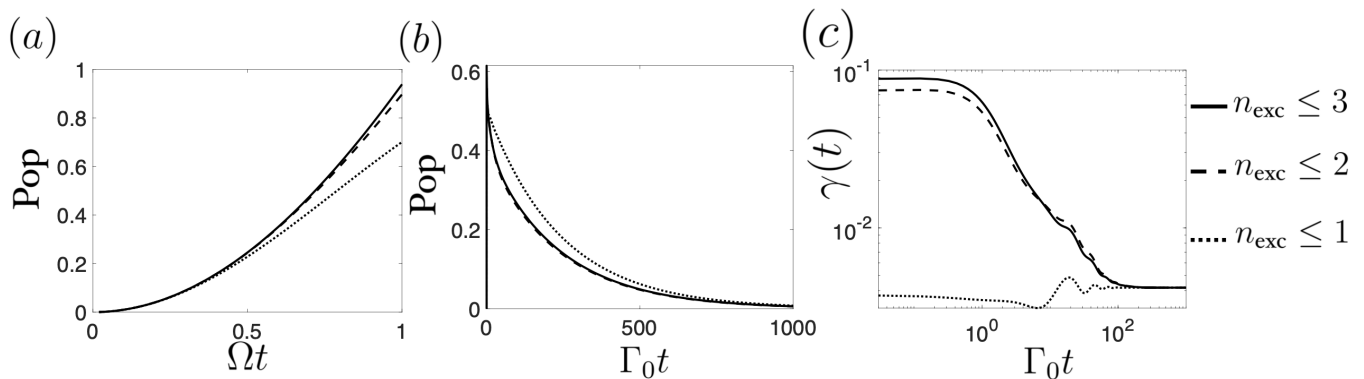


FIG. 10. a) Total atomic population in the chain for a numerical truncation of the M.E up to  $n_{\text{exc}} = 1$  (black dotted), 2 (black dashed) and 3 (solid black) during the illumination step in (a) and during the storage step of the protocol in (b). The numerical parameters are  $N = 10$ ,  $a/\lambda_{eg} = 0.35$ ,  $\Omega = 100\Gamma_0$ ,  $\Delta = 100\Gamma_0$ ,  $\Omega t_1 = 0.8$  and the polarization of the atoms is parallel to the chain. In (c) the origin of time is taken at the beginning of the storage ( $t = t_2$ ).

decay rates:  $\kappa = \Gamma_{\xi=(1,2)}^{(2)}/\Gamma_{\xi=1}^{(1)}$ . In Fig. 9, we plot its numerical value as a function of  $N$  and  $a/\lambda_{eg}$ . In the regime where both modes are subradiant,  $\kappa$  is found to be almost constant to a value around 9.

#### Appendix E: Justification of the truncation of the Hilbert space to $n_{\text{exc}} \leq 2$ in the nonlinear regime

In this appendix we justify the validity of the numerical truncation of the Hilbert space up to  $n_{\text{exc}} \leq 2$  for the study of the total population and the instantaneous decay rate. In Fig. 10(a,b) we plot the total population in the chain computed with a numerical truncation of the Hilbert space going from  $n_{\text{exc}} \leq 1$  to  $n_{\text{exc}} \leq 3$  (in black solid, dashed and pointed lines). Let us denote  $\text{Pop}_{n_{\text{exc}}}$  the total population computed with a numerical truncation up to  $n_{\text{exc}}$ . We observe that  $\text{Pop}_2$  and  $\text{Pop}_3$  are very similar during the illumination (a) and the storage

(b) steps of the protocol. This demonstrates that the numerical truncation to  $n_{\text{exc}} \leq 2$  is enough to properly represent the total population in the system during the different steps of our protocol in the limit of low three-photon population defined as  $(\Omega t_1)^6 \ll 1$ .

Let us now justify the validity of the numerical truncation to  $n_{\text{exc}} \leq 2$  in the analysis of  $t_{\text{tr}}$ . To do so we plot in Fig. 10(c) the numerical value of  $\gamma(t)$  during the storage computed with a numerical truncation of the Hilbert space from  $n_{\text{exc}} \leq 1$  to  $n_{\text{exc}} \leq 3$ . We see that all curves have the same long time limit (given by the decay rate of the most subradiant singly-excited state). However, it appears that the reduction of the analysis to  $n_{\text{exc}} \leq 1$  creates a strong error in the short time behavior of the instantaneous decay rate. By contrast, comparing  $\gamma(t)$  for  $n_{\text{exc}} \leq 2$  and  $n_{\text{exc}} \leq 3$ , we see that the presence of a three-photon population only slightly modifies the instantaneous decay rate for times shorter than  $t_{\text{tr}}$ . From this analysis, we conclude that we can neglect the tiny three-photon population (and higher manifolds), in the analysis of the  $t_{\text{tr}}$  made in the nonlinear regime.

- 
- [1] K. Hammerer, A. S. Sørensen, and E. S. Polzik, Quantum interface between light and atomic ensembles, *Reviews of Modern Physics* **82**, 1041 (2010).  
 [2] J.-M. Raimond, M. Brune, and S. Haroche, Manipulating quantum entanglement with atoms and photons in a cavity, *Reviews of Modern Physics* **73**, 565 (2001).  
 [3] M. Saffman, T. G. Walker, and K. Mølmer, Quantum information with rydberg atoms, *Reviews of Modern Physics* **82**, 2313 (2010).  
 [4] H. J. Kimble, The quantum internet, *Nature* **453**, 1023 (2008).  
 [5] J. D. Thompson, T. Tiecke, N. P. de Leon, J. Feist, A. Akimov, M. Gullans, A. S. Zibrov, V. Vuletić, and M. D. Lukin, Coupling a single trapped atom to a nanoscale optical cavity, *Science* **340**, 1202 (2013).  
 [6] A. Reiserer and G. Rempe, Cavity-based quantum networks with single atoms and optical photons, *Reviews of Modern Physics* **87**, 1379 (2015).  
 [7] D. Plankensteiner, C. Sommer, H. Ritsch, and C. Genes, Cavity antiresonance spectroscopy of dipole coupled subradiant arrays, *Physical Review Letters* **119**, 093601 (2017).  
 [8] I. Shlesinger, P. Senellart, L. Lanco, and J.-J. Greffet, Time-frequency encoded single-photon generation and broadband single-photon storage with a tunable subradiant state, *Optica* **8**, 95 (2021).  
 [9] M. Lei, R. Fukumori, J. Rochman, B. Zhu, M. Endres, J. Choi, and A. Faraon, Many-body cavity quantum electrodynamics with driven inhomogeneous emitters, *Nature*, 1 (2023).

- [10] K. Nayak, P. Melentiev, M. Morinaga, F. Le Kien, V. Balykin, and K. Hakuta, Optical nanofiber as an efficient tool for manipulating and probing atomic fluorescence, *Optics Express* **15**, 5431 (2007).
- [11] P. Solano, P. Barberis-Blostein, F. K. Fatemi, L. A. Orozco, and S. L. Rolston, Super-radiance reveals infinite-range dipole interactions through a nanofiber, *Nature communications* **8**, 1 (2017).
- [12] N. V. Corzo, J. Raskop, A. Chandra, A. S. Sheremet, B. Gouraud, and J. Laurat, Waveguide-coupled single collective excitation of atomic arrays, *Nature* **566**, 359 (2019).
- [13] R. Pennetta, M. Blaha, A. Johnson, D. Lechner, P. Schneeweiss, J. Volz, and A. Rauschenbeutel, Collective radiative dynamics of an ensemble of cold atoms coupled to an optical waveguide, *Physical Review Letters* **128**, 073601 (2022).
- [14] A. Goban, C.-L. Hung, S.-P. Yu, J. Hood, J. Muniz, J. Lee, M. Martin, A. McClung, K. Choi, D. E. Chang, *et al.*, Atom–light interactions in photonic crystals, *Nature communications* **5**, 1 (2014).
- [15] A. Goban, C.-L. Hung, J. Hood, S.-P. Yu, J. Muniz, O. Painter, and H. Kimble, Superradiance for atoms trapped along a photonic crystal waveguide, *Physical Review Letters* **115**, 063601 (2015).
- [16] P. Lodahl, S. Mahmoodian, and S. Stobbe, Interfacing single photons and single quantum dots with photonic nanostructures, *Reviews of Modern Physics* **87**, 347 (2015).
- [17] S.-P. Yu, J. Hood, J. Muniz, M. Martin, R. Norte, C.-L. Hung, S. M. Meenehan, J. D. Cohen, O. Painter, and H. Kimble, Nanowire photonic crystal waveguides for single-atom trapping and strong light-matter interactions, *Applied Physics Letters* **104**, 111103 (2014).
- [18] N. Fayard, A. Bouscal, J. Berroir, A. Urvoy, T. Ray, S. Mahapatra, M. Kemiche, J. A. Levenson, J.-J. Greffet, K. Bencheikh, J. Laurat, and C. Sauvan, Asymmetric comb waveguide for strong interactions between atoms and light, *Opt. Express* **30**, 45093 (2022).
- [19] A. Bouscal, M. Kemiche, S. Mahapatra, N. Fayard, J. Berroir, T. Ray, J.-J. Greffet, F. Raineri, A. Levenson, K. Bencheikh, *et al.*, Systematic design of a robust half-w1 photonic crystal waveguide for interfacing slow light and trapped cold atoms, arXiv preprint arXiv:2301.04675 (2023).
- [20] Q. A. Turchette, C. J. Hood, W. Lange, H. Mabuchi, and H. J. Kimble, Measurement of conditional phase shifts for quantum logic, *Physical Review Letters* **75**, 4710 (1995).
- [21] D. E. Chang, V. Vuletić, and M. D. Lukin, Quantum nonlinear optics—photon by photon, *Nature Photonics* **8**, 685 (2014).
- [22] D. Roy, C. M. Wilson, and O. Firstenberg, Colloquium: Strongly interacting photons in one-dimensional continuum, *Reviews of Modern Physics* **89**, 021001 (2017).
- [23] A. S. Sheremet, M. I. Petrov, I. V. Iorsh, A. V. Poshakinskiy, and A. N. Poddubny, Waveguide quantum electrodynamics: collective radiance and photon-photon correlations, *Reviews of Modern Physics* **95**, 015002 (2023).
- [24] R. J. Bettles, S. A. Gardiner, and C. S. Adams, Enhanced optical cross section via collective coupling of atomic dipoles in a 2d array, *Physical Review Letters* **116**, 103602 (2016).
- [25] G. Facchinetti, S. D. Jenkins, and J. Ruostekoski, Storing light with subradiant correlations in arrays of atoms, *Physical Review Letters* **117**, 243601 (2016).
- [26] E. Shahmoon, D. S. Wild, M. D. Lukin, and S. F. Yelin, Cooperative resonances in light scattering from two-dimensional atomic arrays, *Physical Review Letters* **118**, 113601 (2017).
- [27] J. Rui, D. Wei, A. Rubio-Abadal, S. Hollerith, J. Zeiher, D. M. Stamper-Kurn, C. Gross, and I. Bloch, A subradiant optical mirror formed by a single structured atomic layer, *Nature* **583**, 369 (2020).
- [28] R. H. Dicke, Coherence in spontaneous radiation processes, *Physical review* **93**, 99 (1954).
- [29] M. Gross and S. Haroche, Superradiance: An essay on the theory of collective spontaneous emission, *Physics reports* **93**, 301 (1982).
- [30] M. O. Scully, E. S. Fry, C. R. Ooi, and K. Wódkiewicz, Directed spontaneous emission from an extended ensemble of  $n$  atoms: Timing is everything, *Physical Review Letters* **96**, 010501 (2006).
- [31] M. O. Araújo, I. Krešić, R. Kaiser, and W. Guerin, Superradiance in a large and dilute cloud of cold atoms in the linear-optics regime, *Physical Review Letters* **117**, 073002 (2016).
- [32] Y. He, L. Ji, Y. Wang, L. Qiu, J. Zhao, Y. Ma, X. Huang, S. Wu, and D. E. Chang, Atomic spin-wave control and spin-dependent kicks with shaped subnanosecond pulses, *Physical Review Research* **2**, 043418 (2020).
- [33] Y. He, L. Ji, Y. Wang, L. Qiu, J. Zhao, Y. Ma, X. Huang, S. Wu, and D. E. Chang, Geometric control of collective spontaneous emission, *Physical Review Letters* **125**, 213602 (2020).
- [34] A. Rastogi, E. Saglamyurek, T. Hrushevskyi, and L. J. LeBlanc, Superradiance-mediated photon storage for broadband quantum memory, *Physical Review Letters* **129**, 120502 (2022).
- [35] M. O. Scully, Single photon subradiance: quantum control of spontaneous emission and ultrafast readout, *Physical Review Letters* **115**, 243602 (2015).
- [36] D. Plankensteiner, L. Ostermann, H. Ritsch, and C. Genes, Selective protected state preparation of coupled dissipative quantum emitters, *Scientific reports* **5**, 1 (2015).
- [37] W. Guerin, M. O. Araújo, and R. Kaiser, Subradiance in a large cloud of cold atoms, *Physical Review Letters* **116**, 083601 (2016).
- [38] A. Cipris, N. A. Moreira, T. do Espírito Santo, P. Weiss, C. Villas-Boas, R. Kaiser, W. Guerin, and R. Bachelard, Subradiance with saturated atoms: population enhancement of the long-lived states, *Physical Review Letters* **126**, 103604 (2021).
- [39] G. Ferioli, A. Glicenstein, L. Henriët, I. Ferrier-Barbut, and A. Browaeys, Storage and release of subradiant excitations in a dense atomic cloud, *Physical Review X* **11**, 021031 (2021).
- [40] I. Bloch, J. Dalibard, and S. Nascimbene, Quantum simulations with ultracold quantum gases, *Nature Physics* **8**, 267 (2012).
- [41] F. Nogrette, H. Labuhn, S. Ravets, D. Barredo, L. Béguin, A. Vernier, T. Lahaye, and A. Browaeys, Single-atom trapping in holographic 2d arrays of microtraps with arbitrary geometries, *Physical Review X* **4**, 021034 (2014).
- [42] M. Endres, H. Bernien, A. Keesling, H. Levine, E. R. Anschuetz, A. Krajenbrink, C. Senko, V. Vuletić, M. Greiner, and M. D. Lukin, Atom-by-atom assembly

- of defect-free one-dimensional cold atom arrays, *Science* **354**, 1024 (2016).
- [43] D. Barredo, S. De Léséleuc, V. Lienhard, T. Lahaye, and A. Browaeys, An atom-by-atom assembler of defect-free arbitrary two-dimensional atomic arrays, *Science* **354**, 1021 (2016).
- [44] K. Srakaew, P. Weckesser, S. Hollerith, D. Wei, D. Adler, I. Bloch, and J. Zeiher, A subwavelength atomic array switched by a single rydberg atom, *Nature Physics*, 1 (2023).
- [45] K. Ballantine and J. Ruostekoski, Quantum single-photon control, storage, and entanglement generation with planar atomic arrays, *PRX Quantum* **2**, 040362 (2021).
- [46] O. Rubies-Bigorda, V. Walther, T. L. Patti, and S. F. Yelin, Photon control and coherent interactions via lattice dark states in atomic arrays, *Physical Review Research* **4**, 013110 (2022).
- [47] M. Norcia, A. Young, and A. Kaufman, Microscopic control and detection of ultracold strontium in optical-tweezer arrays, *Physical Review X* **8**, 041054 (2018).
- [48] S. Sashkin, J. Wilson, B. Grinkemeyer, and J. Thompson, Narrow-line cooling and imaging of ytterbium atoms in an optical tweezer array, *Physical Review Letters* **122**, 143002 (2019).
- [49] S. de Léséleuc, D. Barredo, V. Lienhard, A. Browaeys, and T. Lahaye, Optical control of the resonant dipole-dipole interaction between rydberg atoms, *Physical Review Letters* **119**, 053202 (2017).
- [50] J. Ville, T. Bienaimé, R. Saint-Jalm, L. Corman, M. Aidelsburger, L. Chomaz, K. Kleinlein, D. Perconte, S. Nascimbène, J. Dalibard, *et al.*, Loading and compression of a single two-dimensional bose gas in an optical accordion, *Physical Review A* **95**, 013632 (2017).
- [51] M. Reitz, C. Sommer, and C. Genes, Cooperative quantum phenomena in light-matter platforms, *PRX Quantum* **3**, 010201 (2022).
- [52] G. S. Agarwal, *Quantum optics* (Cambridge University Press, 2012).
- [53] A. Asenjo-Garcia, M. Moreno-Cardoner, A. Albrecht, H. Kimble, and D. E. Chang, Exponential improvement in photon storage fidelities using subradiance and “selective radiance” in atomic arrays, *Physical Review X* **7**, 031024 (2017).
- [54] M. Manzoni, M. Moreno-Cardoner, A. Asenjo-Garcia, J. V. Porto, A. V. Gorshkov, and D. Chang, Optimization of photon storage fidelity in ordered atomic arrays, *New journal of physics* **20**, 083048 (2018).
- [55] Y.-X. Zhang and K. Mølmer, Theory of subradiant states of a one-dimensional two-level atom chain, *Physical Review Letters* **122**, 203605 (2019).
- [56] Y.-X. Zhang and K. Mølmer, Subradiant emission from regular atomic arrays: Universal scaling of decay rates from the generalized bloch theorem, *Physical Review Letters* **125**, 253601 (2020).
- [57] D. Chang, J. Douglas, A. González-Tudela, C.-L. Hung, and H. Kimble, Colloquium: Quantum matter built from nanoscopic lattices of atoms and photons, *Reviews of Modern Physics* **90**, 031002 (2018).
- [58] Y.-X. Zhang, C. Yu, and K. Mølmer, Subradiant bound dimer excited states of emitter chains coupled to a one dimensional waveguide, *Physical Review Research* **2**, 013173 (2020).
- [59] R. J. Bettles, M. D. Lee, S. A. Gardiner, and J. Ruostekoski, Quantum and nonlinear effects in light transmitted through planar atomic arrays, *Communications Physics* **3**, 141 (2020).
- [60] M. Moreno-Cardoner, D. Goncalves, and D. E. Chang, Quantum nonlinear optics based on two-dimensional rydberg atom arrays, *Physical Review Letters* **127**, 263602 (2021).
- [61] N. Fayard, L. Henriët, A. Asenjo-Garcia, and D. Chang, Many-body localization in waveguide quantum electrodynamics, *Physical Review Research* **3**, 033233 (2021).
- [62] R. Holzinger, R. Gutiérrez-Jáuregui, T. Hönl-Deerinis, G. Kirchmair, A. Asenjo-Garcia, and H. Ritsch, Control of localized single-and many-body dark states in waveguide qed, *Physical Review Letters* **129**, 253601 (2022).
- [63] S. J. Masson, I. Ferrier-Barbut, L. A. Orozco, A. Browaeys, and A. Asenjo-Garcia, Many-body signatures of collective decay in atomic chains, *Physical Review Letters* **125**, 263601 (2020).
- [64] A. Cidrim, T. do Espirito Santo, J. Schachenmayer, R. Kaiser, and R. Bachelard, Photon blockade with ground-state neutral atoms, *Physical Review Letters* **125**, 073601 (2020).
- [65] L. Williamson, M. O. Borgh, and J. Ruostekoski, Superatom picture of collective nonclassical light emission and dipole blockade in atom arrays, *Physical review letters* **125**, 073602 (2020).
- [66] L. Zhang, V. Walther, K. Mølmer, and T. Pohl, Photon-photon interactions in rydberg-atom arrays, *Quantum* **6**, 674 (2022).
- [67] S. Richter, S. Wolf, J. von Zanthier, and F. Schmidt-Kaler, Collective photon emission of two correlated atoms in free space, *Physical Review Research* **5**, 013163 (2023).
- [68] L. Henriët, J. S. Douglas, D. E. Chang, and A. Albrecht, Critical open-system dynamics in a one-dimensional optical-lattice clock, *Physical Review A* **99**, 023802 (2019).
- [69] O. Rubies-Bigorda, S. Ostermann, and S. F. Yelin, Dynamic population of multiexcitation subradiant states in incoherently excited atomic arrays, *Physical Review A* **107**, L051701 (2023).
- [70] L. Ostermann, H. Ritsch, and C. Genes, Protected state enhanced quantum metrology with interacting two-level ensembles, *Physical Review Letters* **111**, 123601 (2013).
- [71] G. Facchinetti and J. Ruostekoski, Interaction of light with planar lattices of atoms: Reflection, transmission, and cooperative magnetometry, *Physical Review A* **97**, 023833 (2018).
- [72] D. S. Wild, E. Shahmoon, S. F. Yelin, and M. D. Lukin, Quantum nonlinear optics in atomically thin materials, *Physical Review Letters* **121**, 123606 (2018).
- [73] P.-O. Guimond, A. Grankin, D. Vasilyev, B. Vermersch, and P. Zoller, Subradiant bell states in distant atomic arrays, *Physical Review Letters* **122**, 093601 (2019).
- [74] R. Bekenstein, I. Pikovski, H. Pichler, E. Shahmoon, S. F. Yelin, and M. D. Lukin, Quantum metasurfaces with atom arrays, *Nature Physics* **16**, 676 (2020).
- [75] A. S. Solntsev, G. S. Agarwal, and Y. S. Kivshar, Metasurfaces for quantum photonics, *Nature Photonics* **15**, 327 (2021).
- [76] S. J. Masson and A. Asenjo-Garcia, Atomic-waveguide quantum electrodynamics, *Physical Review Research* **2**, 043213 (2020).